Fusion Engineering and Design 202 (2024) 114306

Contents lists available at ScienceDirect

Fusion Engineering and Design

journal homepage: www.elsevier.com/locate/fusengdes

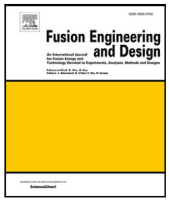

Experimental investigation of MHD flows in a WCLL TBM mock-up

C. Courtessole *, H.-J. Brinkmann, L. Bühler, J. Roth

Karlsruhe Institute of Technology, Postfach 3640, 76021 Karlsruhe, Germany

ARTICLE INFO

Keywords:
Magnetohydrodynamics (MHD)
Water-cooled lead-lithium (WCLL) blanket
MHD pressure drop measurements

ABSTRACT

Experiments have been performed in the MEKKA laboratory of the Karlsruhe Institute of Technology to characterize the influence of a magnetic field on liquid metal flows in a scaled mock-up of the water-cooled lead-lithium test blanket module of ITER. The test section consists of eight breeder units that are fed and drained by long electrically coupled manifolds oriented along the poloidal direction. Pressure differences between several points of the mock-up have been recorded for various liquid metal flow rates and strengths of the imposed magnetic field. The main contributions to the total pressure drop in the test section have been identified as a function of characteristic flow parameters. For sufficiently strong magnetic fields, the experimental data shows that the non-dimensional pressure loss is practically independent of the flow rate, i.e. inertia forces become negligible. The experiments also confirm previous conclusions of magnetohydrodynamic experiments performed in a scaled-down mock-up of a helium-cooled lead-lithium blanket, namely that the largest pressure drop in the blanket module originates from the flow in the distributing and collecting manifolds. Moreover, the experimental study demonstrates that the current manifold design does not allow the flow to be uniformly distributed among all the breeder units.

1. Introduction

The European development strategy for DEMO breeding blankets has recently been revised in favor of a more synergetic approach with the EU ITER test blanket module (TBM) program [1]. The new strategy comes with a renewed focus on the water-cooled lead-lithium (WCLL) concept, which has been identified as one of the two reference candidates for DEMO and selected for tests in ITER. The WCLL TBM, which will be installed in one of the equatorial ports of ITER, is being designed to exhibit the same features as the European DEMO WCLL breeding blanket currently considered [2]. It uses Reduced Activation Ferritic-Martensitic (RAFM) steel as a structural material, and it relies on liquid lead-lithium alloy (PbLi) as a neutron multiplier and tritium breeder, and pressurized water as a coolant.

A preliminary design of the WCLL TBM has been described in [3] and is shown in Fig. 1. It consists of 16 breeding units (BU) arranged in two columns of 8 BUs stacked on top of one another along the poloidal direction. Each column includes its own feeding and draining liquid metal manifolds to which BUs connect through rectangular openings (windows) in their back plates. All BUs encompass a number of water-cooled double-walled tubes oriented in radial–toroidal planes for heat removal. These pipes cross the liquid metal manifolds to reach a shared back plate to which they are welded. The cooling tubes and the stiffening plates protruding into the manifolds obstruct the liquid metal flow, and lead to tortuous and complex 3D flow paths with locally increased velocity.

Three-dimensional flows of electrically conducting fluids in strong magnetic fields are known to suffer from intense magnetohydrodynamic (MHD) effects responsible for additional pressure drop and peculiar flow patterns [4]. Additionally, large velocity in the manifolds resulting from their much smaller cross-sections compared to the combined ones of the breeder units are expected to generate most of the pressure drop of the module, as shown by past experiments in a helium-cooled lead-lithium (HCLL) TBM mock-up [5,6]. Furthermore, the geometry of the manifolds have also been proven to influence flow partitioning across the various breeding modules [7,8].

Since the complexity of the WCLL geometry still represents a challenging task to examine 3D MHD effects occurring in the whole TBM through numerical simulations [9], experiments happen to be essential to investigate MHD flows at the scale of an entire module. In order to study the pressure and flow distributions in the WCLL TBM, a scaled-down mock-up was designed and fabricated at KIT. The module was instrumented to measure pressure differences between remarkable

* Corresponding author.
E-mail address: cyril.courtessole@kit.edu (C. Courtessole).

https://doi.org/10.1016/j.fusengdes.2024.114306
Received 11 October 2023; Received in revised form 8 February 2024; Accepted 1 March 2024
Available online 27 March 2024

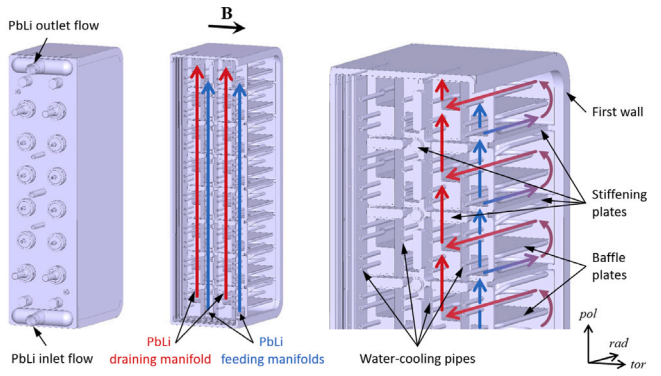

Fig. 1. Design of the WCLL TBM [3]. Internal details such as the liquid metal manifolds, double-walled water tubes and breeder units can be observed.

points of the geometry. Data were collected for several liquid metal flow rates and strengths of the external magnetic field.

2. Experimental set-up

In a fusion environment, liquid metal flows are characterized by their large Hartmann numbers and by their Reynolds numbers serving, respectively, as a nondimensional measure of the strength of the imposed magnetic field and of the flow velocity

$$Ha = BL\sqrt{\frac{\sigma}{\rho\nu}},\ Re = \frac{uL}{\nu},$$

with ρ, ν, and σ denoting the liquid metal density, kinematic viscosity, and specific electric conductivity, respectively. B is the strength of the magnetic field, and u and L are the velocity and length scale of the problem.

Here, the typical scales have been chosen related to the breeder units using the half of the internal toroidal size of the breeding zone as a characteristic length, i.e. $L_{\mathrm{BU}} = 39$ mm in the mock-up, and the average mean velocity in a single BU is

$$u_{\mathrm{BU}} = \frac{Q/8}{A_{\mathrm{BU}}/2}$$

where Q is the total volumetric flow rate entering the mock-up that is distributed over 8 BUs of cross-section $A_{\mathrm{BU}}/2$. The factor $1/2$ accounts for the fact that the liquid metal first moves towards the first wall in one part of the breeder unit before coming back in the remaining fraction of the same unit.

Experiments have been performed in the MEKKA laboratory at KIT using eutectic sodium–potassium (NaK) as a model fluid [10]. This liquid metal has the advantage of being liquid at room temperature, and its physical properties - in particular its high electrical conductivity and low density compared to PbLi - enable laboratory experiments to be performed at characteristic flow parameters of the same order of magnitude as ones occurring in a fusion reactor ($Ha \sim 10^4$) despite a maximum magnetic field limited to 2.1 T in the laboratory. In the present study, it is possible to reach typical values of $500 \leq Ha \leq 4000$ and $0 \leq Re \leq 5500$, the maximum value of the Reynolds number being dependent on the overall pressure drop of the mock-up and therefore on the strength of the imposed transverse magnetic field.

2.1. Scaled WCLL TBM mock-up

In order to fit within the limited space of the dipole magnet inside which the magnetic field is uniform, i.e. in an 800 mm × 480 mm × 168 mm volume, the geometry of the mock-up was adapted from the ITER TBM design described in [3]. Since the manifolds have been identified to contribute the most to the pressure drop, it is critical to replicate these components identically in the test section. Moreover, to perform experiments at meaningful parameters, the characteristic length of the manifolds along the magnetic field direction has to be as large as possible. Therefore, only half of the TBM geometry, namely one set of manifolds and eight breeder units, is considered for the experiments.

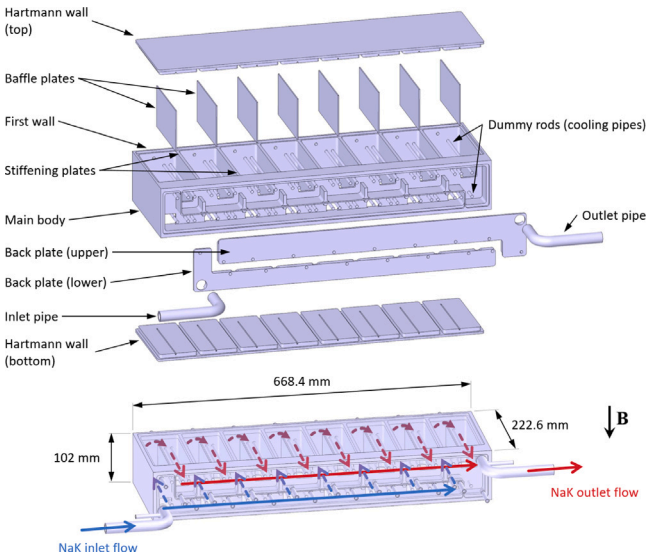

Fig. 2. Exploded view of the WCLL TBM mock-up (top) and internal view showing the liquid metal flow paths inside the WCLL TBM mock-up (bottom).

The final mock-up design is shown in Fig. 2. It is obtained by scaling down the TBM by a factor of 2.5 and has external dimensions of 668.4 mm × 222.6 mm × 102.0 mm. The test section is made of austenite stainless steel (1.4571) that is non-magnetic to avoid distortion of the imposed external magnetic field. Its design has been simplified from the original ITER TBM configuration to facilitate manufacturing and reduce fabrication costs. Most of the modifications result from discarding details related to the water flow in the module. The cooling channels inside the walls were omitted, which is a reasonable approximation for MHD experiments as long as the thickness of the wall of the mock-up is adjusted to maintain a wall electric conductance comparable to the real design. In addition, the C-shaped cooling pipes immersed in the breeding zone are replaced by two radial dummy rods simulating obstacles of the same size. This design choice enables the main body of the mock-up to be milled from a single block (see Fig. 2), thereby reducing the number of parts and welds in the assembly. Finally, the back plates constituting the water distributor and collector are also ignored. Further details related to the design and fabrication of the mock-up can be found in [11].

Despite these discrepancies with the reference WCLL TBM design, the mock-up retains high geometric similarity with the original concept to allow for meaningful MHD phenomenon to be investigated. The liquid metal enters into the mock-up through a circular pipe. It then expands into the feeding manifold that distributes the flow to eight breeder units through a long poloidal channel that is electrically coupled with the neighboring collector. The fluid flows in each unit through a rectangular opening in the back plate of the supply manifold. It continues radially towards the first wall, turns around the baffle plate, and is redirected to the outlet manifold into which it flows via another rectangular window. It then exits the mock-up via another circular pipe located downstream of the collector as seen at the bottom of Fig. 2.

2.2. Differential pressure measurement system

The mock-up is equipped with 28 pressure taps distributed along the liquid metal flow paths, including nine on the back plate of each

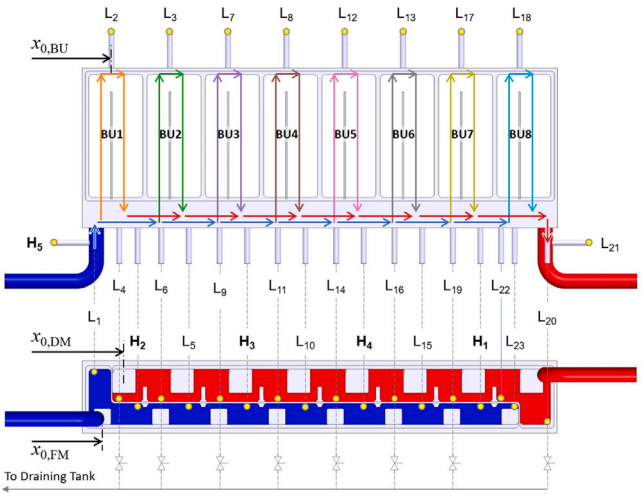

Fig. 3. Location of the pressure taps and visualization of typical flow paths in the mock-up. Pressure taps labeled H_i and L_k are connected to the high-, respectively low-, pressure side of the differential pressure transducers.

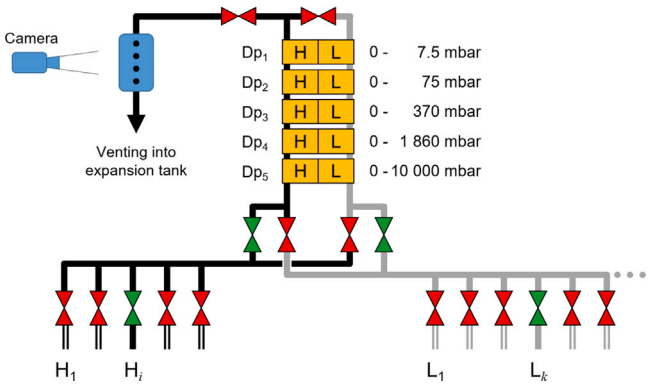

Fig. 4. Architecture of the differential pressure measurement system showing how pressure taps H_i and L_k are connected to the capacitive pressure transducers.

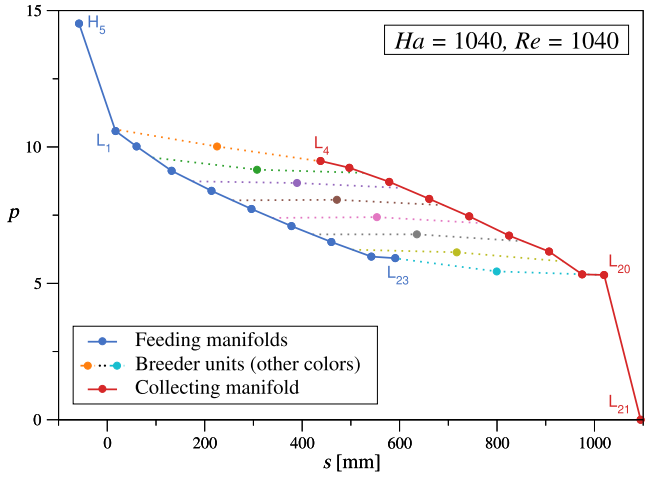

Fig. 5. Nondimensional pressure distribution along typical flow paths in the blanket module for $Ha = 1040$ and $Re = 1040$. The main contributions to the total pressure drop occur in the inlet/outlet pipes and in the manifolds ($H_5 - L_{23}$ shown in blue, and $L_4 - L_{21}$ displayed in red).

manifold, and one on the first wall of each breeder unit. Additionally, two extra pressure taps (H_5 and L_{21}) are welded on the inlet and outlet circular pipes of the mock-up (see Fig. 3). To avoid installing additional venting lines on the test section, the pressure pipes have been placed at the highest points of the breeder units and feeding manifold. Similarly, the mock-up can be completely drained by gravity via its main supply pipe and the eight pressure taps positioned at the lower extremity of the collecting manifold and insulated from the draining tank of the loop by manual valves as seen in Fig. 3.

The pressure lines are connected to a differential pressure measurement system located outside the magnet via an array of valves that are associated with five capacitive pressure sensors (Fig. 4). The valves are pneumatically actuated and controlled remotely via a computer. All five uni-polar pressure transducers are mounted in series such that they are all sensing the same positive pressure difference $\Delta p_{ik} = p_{H_i} - p_{L_k}$ between their high- and low-pressure side to which the pressure lines $H_{i=1\ldots5}$ and $L_{k=1\ldots24}$ are connected, respectively. This setup allows for very accurate measurements over a broad span of pressures thanks to the staggered overlapping ranges of the sensors extending from a few mbars to 10 bars. The retained pressure difference is determined from the readings of all the sensors weighted according to their measuring range such that the transducer with the highest precision contributes the most to the final result, and those that are out of range are ignored. During the experiment, pressure line valves are switched automatically according to a predefined measuring sequence to record pressure differences between selected pressure taps. The system also includes a set of valves to reverse the polarity of the measurement, should the pressure at line L_k becomes larger than that at line H_i.

Prior to collecting data, all measuring lines are carefully vented to ensure no residual argon gas is trapped in the pressure sensors, valves, or pressure pipes. This step is critical as any gas bubbles would create measurement errors caused by the Laplace pressure due to the surface tension of the liquid metal-gas interface. To guarantee the correct venting of the system, NaK is pumped through every individual pressure line until an uninterrupted stream of liquid metal is seen falling into the expansion tank.

3. Results

In the following, the pressure distribution throughout the entire mock-up has been reconstructed from pressure differences measured between various pressure taps. Results are plotted along the curvilinear coordinate s that represents the length along typical flow paths depicted in Fig. 3 starting from the inlet of the supply manifold ($s = 0$). For a universal nondimensional representation of the results, the pressure data is scaled by the characteristic pressure value p_M for the manifolds.

$$p_M = \sigma u_M L_M B^2.$$

In the manifolds, the typical length scale is only half of that in the breeder units $L_M = {}^{L_{BU}}/_2$ due to the presence of the baffle plate separating both manifolds, and the characteristic velocity may be defined as $u_M = {}^{Q}/_{A_M}$ where the cross-section A_M accounts for both distributing and collecting manifolds since the entire flow rate of liquid metal is carried by both manifolds at any poloidal location.

Fig. 5 shows a pressure distribution representative of the MHD flow obtained for $Ha = 1040$ and $Re = 1040$. The main contributions to the total pressure drop in the mock-up, $\Delta p_{tot} = p_{H_5} - p_{L_{21}}$, occur in the inlet and outlet circular pipes as the flow expands, or contracts, as it respectively enters or exits the test section, $\Delta p_{in} = p_{H_5} - p_{L_1}$ and $\Delta p_{out} = p_{L_{20}} - p_{L_{21}}$, as well as in the feeding and draining manifolds, $\Delta p_{FM} = p_{L_1} - p_{L_{23}}$ and $\Delta p_{DM} = p_{L_4} - p_{L_{20}}$. These large pressure drops are mostly caused by the reduced cross-section of these elements that lead to high velocities of liquid metal. Comparatively, the pressure drops inside the breeder units are very small as the fluid moves more than

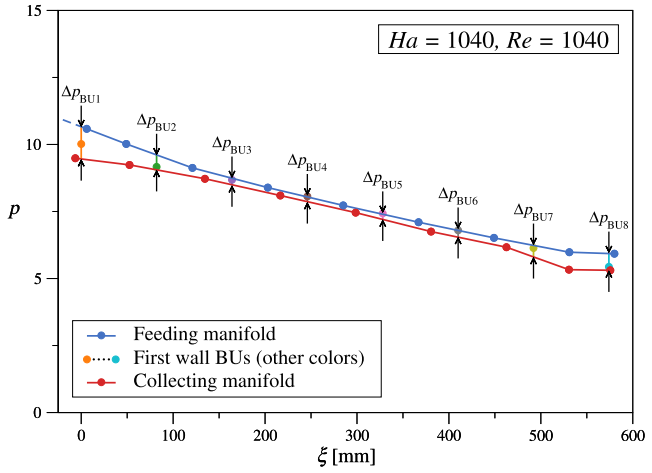

Fig. 6. Nondimensional pressure distribution $p(\xi)$ along the poloidal coordinate ξ for $Ha = 1040$ and $Re = 1040$. Blue line and symbols refer to the feeding manifold, red line and symbols to the draining manifolds, and color lines between arrow tips represent the driving pressure difference between the feeding and draining manifolds in each BU. The recorded pressure values at the pressure taps are shown as dots.

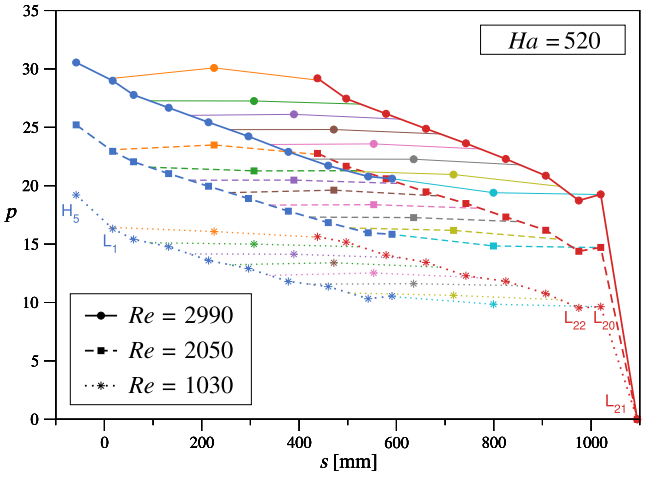

Fig. 7. Comparison of pressure distributions along typical flow paths in the blanket module for $Ha \simeq 520$ and three Reynolds numbers $Re \simeq 1030$, 2050, and 2990.

an order of magnitude slower there than in the manifolds ($u_{BU}/u_M = A_M/4A_{BU} \simeq 1/12$).

For each breeder unit, the driving pressure difference can be estimated by interpolating pressures at the centers of the rectangular openings in the supplying and collecting manifolds from pressure values of neighboring pressure taps (dots in Fig. 6). Results are presented in Fig. 6 along the poloidal coordinate $\xi = x - x_0$, the origins of which (see Fig. 3) are chosen at the centers of first windows of feeding ($x_{0,FM}$) and draining ($x_{0,DM}$) manifolds, or at the pressure tap L_2 on the first wall of BU1 for breeder units ($x_{0,BU}$). With such choice, results can be presented with respect to a unique poloidal coordinate associated with each breeder unit.

One can note from Fig. 6 that Δp_{BU} is not the same for all breeder units. It can be seen that the first (BU1 and BU2) and last (BU7 and BU8) units exhibit much larger driving pressure differences than the others (BU3 to BU6). This result suggests that the flow is not uniformly distributed among all breeder units. Instead, external breeder units carry a significantly larger portion of the flow than the central elements similar to what has already been seen in a past investigation for a helium-cooled lead lithium blanket mock-up [12].

The disparity of flow rates between breeder units can be attributed to the geometry of the distributor and collector whose constant cross-sections along the poloidal direction leads to variation of velocity, and therefore of pressure loss, as the flow progresses through the manifolds. In the feeding manifold, a larger pressure drop occurs near the inlet of the manifold where the velocity is higher whereas lower flow rate, i.e. velocity, close to the end of the manifold results in smaller pressure drop. In the collecting manifold, the situation is the opposite. The velocity, thus the pressure drop, increases along the poloidal direction. The resulting pressure profiles in the manifolds cause the driving pressure differences to be nonuniform among the breeder units, which in turn leads to unequal flow partitioning.

Moreover, one can also observe an asymmetry between the first and last breeder units with a larger pressure drop in BU1 than in BU8, $\Delta p_{BU1} > \Delta p_{BU8}$, signaling that most of the flow passes from the feeding to the draining manifold via the first breeder unit. This can be explained by the different cross-sectional areas of the two manifolds. Since the draining manifold is larger than the feeding one, the liquid metal preferentially flows through BU1 to reach sooner the larger draining manifold, where it meets less magnetohydrodynamic resistance.

Experiments performed at smaller Hartmann numbers highlight the influence of inertial effects on the pressure distribution in the mock-up by comparing results obtained for various Reynolds numbers. As displayed in Fig. 7, those become very obvious at the lowest Hartmann number investigated ($Ha \simeq 500$) where the total pressure drop Δp_{tot} is roughly multiplied by 1.5 when the Reynolds number increases from about 1000 to approximately 3000. Inertial effects are especially prominent at the exit of the mock-up where the cross-section suddenly contracts as the liquid metal flows out of the draining manifold through the smaller circular pipe. The influence of the Reynolds number can also be noticed downstream of the collecting manifold where pressure recovery is observed between pressure taps L_{22} and L_{20} as the flow expands at the end of the collecting manifolds. In the breeder units, inertia effects are visible at both ends of the module with an increased pressure loss seen in BU8 when the Reynolds number increases, and some pressure recovery observed in BU1 for $Re \simeq 2000$ and 3000.

As the strength of the magnetic field increases, the effect of inertia becomes weaker as demonstrated in Fig. 8 where pressure distributions are plotted for $Ha = 2100$ and for $Re = 200$, 400, and 840. At such a strong magnetic field, it can be seen that the total pressure drop and the pressure distributions become almost independent of the flow rate of liquid metal in the mock-up. The only small influence of inertia forces on the pressure profiles is visible at the exit of the test section, where the flow suddenly contracts to flow through the circular pipe downstream of the collecting manifold. Aside from that relatively weak effect, it is interesting to note that the pressure drop occurring at the connection of the inlet pipe with the distributing manifold, $\Delta p_{in} = p_{H_5} - p_{L_1}$, is about the same as that seen when the fluid passes from the draining manifold into the outlet pipe, $\Delta p_{out} = p_{L_{20}} - p_{L_{21}}$. This observation suggests that the flow tends to become inertialess, and as such the flow direction no longer matters. Therefore, and since the geometry of the expansion at the inlet of the mock-up is similar than that of the contraction at the exit of the test section, the MHD pressure drop resulting from these variations of cross-section becomes equal. This result also confirms recent computational studies that found less than 2% of deviations in the MHD pressure drop between contraction and expansion flows with a contraction/expansion ratio of 10 in a viscous-electromagnetic flow regime [13].

4. Conclusions

Liquid metal MHD experiments have been performed in the MEKKA laboratory at KIT to investigate pressure drop and flow partitioning in

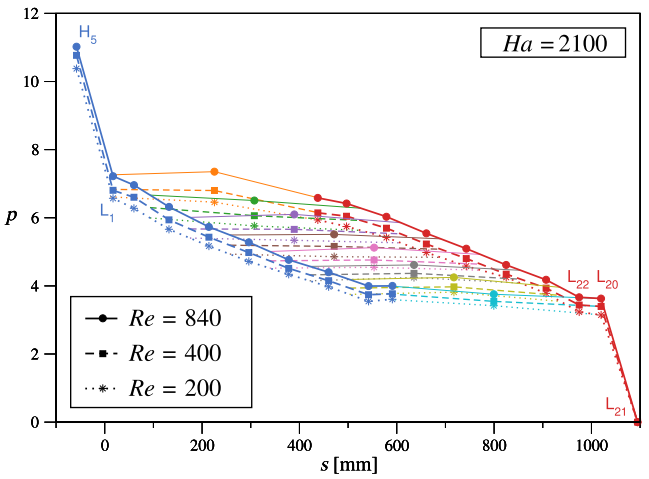

Fig. 8. Comparison of pressure distributions along typical flow paths in the blanket module for $Ha \simeq 2100$ and three Reynolds numbers $Re \simeq 200$, 400, and 840.

manifolds and breeder units of a scaled mock-up for the latest design of a WCLL TBM for ITER. In this parametric study, pressure distributions have been measured for various flow rates (up to $Re = 5500$) and for different strengths of the applied magnetic field in the range $500 \leq Ha \leq 4000$. Results obtained are consistent with previous experimental observations for a HCLL TBM mock-up (see e.g. [6]). It is found that the major fraction of pressure drop occurs in the feeding and draining manifolds while the pressure drop in the breeder units remains relatively small. The largest pressure differences Δp_{BU} between entrances and exits of the breeder units are observed for BU1 and BU8 at both ends of the module. These contributions are significantly larger than for BU2–BU7 so that it is expected that central units will receive much less flow compared to the first and last breeder units. Furthermore, it was observed an asymmetry in the breeder units pressure drops along the poloidal direction, with larger pressure differences in the first breeder unit than in the last one, causing BU1 to receive more flow than BU8. This additional imbalance was found to result from the different cross-section of the feeding and draining manifolds; the feeding manifold cross-section being smaller than that of the draining manifold as predicted in [14].

CRediT authorship contribution statement

C. Courtessole: Data curation, Formal analysis, Investigation, Methodology, Visualization, Writing – original draft. **H.-J. Brinkmann:** Resources. **L. Bühler:** Conceptualization, Supervision, Writing – review & editing. **J. Roth:** Resources.

Declaration of competing interest

The authors declare that they have no known competing financial interests or personal relationships that could have appeared to influence the work reported in this paper.

Data availability

Data will be made available on request.

Acknowledgments

This work has been carried out within the framework of the EUROfusion Consortium, funded by the European Union via the Euratom Research and Training Programme (Grant Agreement No 101052200 — EUROfusion). Views and opinions expressed are however those of the author(s) only and do not necessarily reflect those of the European Union or the European Commission. Neither the European Union nor the European Commission can be held responsible for them.

References

[1] G. Federici, L. Boccaccini, F. Cismondi, M. Gasparotto, Y. Poitevin, I. Ricapito, An overview of the EU breeding blanket design strategy as an integral part of the DEMO design effort, Fusion Eng. Des. 141 (2019) 30–42, http://dx.doi.org/10.1016/j.fusengdes.2019.01.141.

[2] A. Del Nevo, P. Arena, G. Caruso, P. Chiovaro, P.D. Maio, M. Eboli, F. Edemetti, N. Forgione, R. Forte, A. Froio, F. Giannetti, G. Di Gironimo, K. Jiang, S. Liu, F. Moro, R. Mozzillo, L. Savoldi, A. Tarallo, M. Tarantino, A. Tassone, M. Utili, R. Villari, R. Zanino, E. Martelli, Recent progress in developing a feasible and integrated conceptual design of the WCLL BB in EUROfusion project, Fusion Eng. Des. 146 (2019) 1805–1809, http://dx.doi.org/10.1016/j.fusengdes.2019.03.040.

[3] J. Aubert, G. Aiello, D. Alonso, T. Batal, R. Boullon, S. Burles, B. Cantone, F. Cismondi, A. Del Nevo, L. Maqueda, A. Morin, E. Rodríguez, F. Rueda, M. Soldaini, J. Vallory, Design and preliminary analyses of the new water cooled lithium lead TBM for ITER, Fusion Eng. Des. 160 (2020) 111921, http://dx.doi.org/10.1016/j.fusengdes.2020.111921.

[4] S. Smolentsev, R. Moreau, L. Bühler, C. Mistrangelo, MHD thermofluid issues of liquid-metal blankets: Phenomena and advances, Fusion Eng. Des. 85 (2010) 1196–1205, http://dx.doi.org/10.1016/j.fusengdes.2010.02.038.

[5] C. Mistrangelo, L. Bühler, Magnetohydrodynamic pressure drops in geometric elements forming a HCLL blanket mock-up, Fusion Eng. Des. 86 (2011) 2304–2307, http://dx.doi.org/10.1016/j.fusengdes.2011.03.011.

[6] C. Mistrangelo, L. Bühler, H.-J. Brinkmann, Experimental investigation of MHD pressure losses in a mock-up of a liquid metal blanket, Nucl. Fusion 58 (2018) 036012, http://dx.doi.org/10.1088/1741-4326/aaa133.

[7] C. Mistrangelo, L. Bühler, C. Koehly, I. Ricapito, Magnetohydrodynamic velocity and pressure drop in WCLL TBM, Nucl. Fusion 61 (2021) 096037, http://dx.doi.org/10.1088/1741-4326/ac18dc.

[8] L. Bühler, C. Mistrangelo, A simple MHD model for coupling poloidal manifolds to breeder units in liquid metal blankets, Fusion Eng. Des. 191 (2023) 113552, http://dx.doi.org/10.1016/j.fusengdes.2023.113552.

[9] C. Mistrangelo, L. Bühler, V. Klüber, Towards the simulation of MHD flow in an entire WCLL blanket mock-up, Fusion Eng. Des. 193 (2023) 113752, http://dx.doi.org/10.1016/j.fusengdes.2023.113752.

[10] L. Barleon, K.-J. Mack, R. Stieglitz, The MEKKA-Facility a Flexible Tool to Investigate MHD-Flow Phenomena, Tech. Rep. FZKA 5821, Forschungszentrum Karlsruhe, 1996.

[11] C. Koehly, L. Bühler, C. Courtessole, Design of a scaled mock-up of the WCLL TBM for MHD experiments in liquid metal manifolds and breeder units, Fusion Eng. Des. 192 (2023) 113753, http://dx.doi.org/10.1016/j.fusengdes.2023.113753.

[12] L. Bühler, C. Mistrangelo, H.-J. Brinkmann, C. Koehly, Pressure distribution in MHD flows in an experimental test-section for a HCLL blanket, Fusion Eng. Des. 127 (2018) 168–172, http://dx.doi.org/10.1016/j.fusengdes.2018.01.007.

[13] T.J. Rhodes, S. Smolentsev, Pressure drop in a prototypical 3D magnetohydrodynamic flow across contraction of a fusion blanket manifold, J. Nucl. Sci. Technol. 58 (2021) 908–917, http://dx.doi.org/10.1080/00223131.2021.1892550.

[14] L. Bühler, C. Mistrangelo, Geometric optimization of electrically coupled liquid metal manifolds for WCLL blankets, IEEE Trans. Plasma Sci. (2024) http://dx.doi.org/10.1109/TPS.2024.3362689.